

Lattice QCD determination of the normalization of the leading-twist photon distribution amplitude and susceptibility of the quark condensate

S. Bacchio 

*Computation-based Science and Technology Research Center, The Cyprus Institute,
20 Konstantinou Kavafi Street, 2121 Nicosia, Cyprus*

D. Bečirević 

*IJCLab, Pôle Théorie (Bat. 210), CNRS/IN2P3 et Université, Paris-Saclay,
91405 Orsay, France*

G. Gagliardi  and F. Sanfilippo 

*Istituto Nazionale di Fisica Nucleare, Sezione di Roma Tre,
Via della Vasca Navale 84, I-00146 Rome, Italy*



(Received 17 May 2024; accepted 24 June 2024; published 12 August 2024)

The normalization of the leading-twist photon distribution amplitude (DA), f_γ^\perp , is an important ingredient in the study of exclusive processes involving the photon emission by means of QCD sum-rules. In this paper we determine the up-, down- and strange-quark contribution to f_γ^\perp by exploiting its relation to the zero-momentum two-point correlation function of the electromagnetic current J_{em}^μ and the electric component of the tensor current $T^{\mu\nu}$. To that end we employ the gauge ensembles obtained by using $N_f = 2 + 1 + 1$ Wilson-Clover twisted-mass quark flavors, generated by the Extended Twisted Mass (ETM) Collaboration, and after adding all sources of systematic uncertainties, we obtain a total error of 1.5% and 3.5%, respectively, for the light- (u and d) and strange-quark contribution to $f_\gamma^\perp(2 \text{ GeV})$ in the $\overline{\text{MS}}$ scheme, thus improving their accuracy by a factor of 2.3 and 2.8, respectively. For the strange-quark contribution $f_{\gamma,s}^\perp(2 \text{ GeV})$, we observe a discrepancy with respect to previous lattice calculations. By combining our result with the world average lattice value of the chiral condensate, we obtain for the susceptibility of the quark condensate $\chi_d^{\overline{\text{MS}}}(2 \text{ GeV}) \simeq \chi_u^{\overline{\text{MS}}}(2 \text{ GeV}) = 2.17(12) \text{ GeV}^{-2}$.

DOI: [10.1103/PhysRevD.110.034511](https://doi.org/10.1103/PhysRevD.110.034511)

I. INTRODUCTION

QCD sum rules (QCDSR) proved to be an efficient method to get the phenomenologically interesting information about the nonperturbative dynamics of hadrons. For the description of electromagnetic properties of hadrons, including the processes with a photon emission, the authors of Refs. [1,2] modified the standard QCDSR methodology [3] and studied the correlation functions in an external electromagnetic field. From the initial application in computing the nucleon magnetic moments and

the radiative $\Delta \rightarrow p\gamma$ decay rate, the approach has been broadly employed in numerous applications including the hadronic correction to the $Z^*\gamma^*\gamma$ -vertex, entering the electroweak contribution to $(g-2)_\mu$ [4], computation of the neutron electric dipole moment [5,6], studies of chirality violation in the exclusive photoproduction of hard dijets [7], evaluation of the hadronic matrix element of the radiative decays of heavy-light mesons [8,9] as well as many other processes involving the leading-twist photon distribution amplitude (DA) [10–12]. A key nonperturbative quantity needed in this description is the susceptibility of the quark condensate, χ , which measures the response of the chiral condensate to the presence of an external electromagnetic field. As we shall see, it is related to the normalization of the leading-twist photon DA, $f_{\gamma,q}^\perp$, as $f_{\gamma,q}^\perp = \chi_q \langle \bar{q}q \rangle$, where each quantity depends on the renormalization scale in a given

Published by the American Physical Society under the terms of the Creative Commons Attribution 4.0 International license. Further distribution of this work must maintain attribution to the author(s) and the published article's title, journal citation, and DOI. Funded by SCOAP³.

renormalization scheme, and q stands for the (light) quark flavor. It appears that it is more convenient to compute $f_{\gamma,q}^\perp$ directly on the lattice and then combine the result with a known value of $\langle \bar{q}q \rangle^{\overline{\text{MS}}}(2 \text{ GeV})$ [13] to extract $\chi_q^{\overline{\text{MS}}}(2 \text{ GeV})$. The estimate based on the vector meson dominance for the case of lightest flavors in the isospin limit $m_u = m_d \equiv m_\ell^1$ yields $\chi_\ell^{\overline{\text{MS}}}(2 \text{ GeV}) = 1.9(1) \text{ GeV}^{-2}$, in good agreement with the QCDSR result, $\chi_\ell^{\overline{\text{MS}}}(2 \text{ GeV}) = 2.1(2) \text{ GeV}^{-2}$ [10], but both being considerably different from the values advocated in Refs. [16,17]. This situation clearly called for a lattice QCD determination of this quantity. The first such attempts were made in a setup with $N_f = 2$ [18] and $N_f = 2 + 1$ [19] but without accounting for the effects of renormalization. Another attempt was made in Ref. [20], but a detailed lattice QCD study of $f_{\gamma,q}^\perp$ with $N_f = 2 + 1$ staggered quark flavors was performed in Ref. [21], and then considerably improved in Ref. [22] where, in the vanishing quark mass limit, the resulting value of $f_{\gamma,\ell}^\perp(2 \text{ GeV}) = -(45.4 \pm 1.6) \text{ MeV}$ has been quoted. That value then corresponds to $\chi_\ell^{\overline{\text{MS}}}(2 \text{ GeV}) = 2.3(1) \text{ GeV}^{-2}$. In this paper we calculate $f_{\gamma,q}^\perp$, with $q \in \{u, d, s\}$, from the two-point correlation functions computed on the gauge field configurations generated by using the twisted mass QCD on the lattice with $N_f = 2 + 1 + 1$ Wilson-Clover dynamical quarks [23].

The ensembles of gauge field configurations that we use correspond to three lattice spacings $a \in [0.056, 0.08] \text{ fm}$ and the spatial volumes $V = L^3$ with $L \in [5.0, 7.7] \text{ fm}$ [24–27]. After taking the continuum and infinite-volume limits, and by adding all sources of systematic uncertainties in quadrature, we obtain a total error of 1.5% for u, d and 3.5% for the s quark. That represents the improvement by a factor of more than 2 over the previous lattice QCD estimate of these quantities. Our final results in the $\overline{\text{MS}}$ scheme are

$$f_{\gamma,u}^\perp(2 \text{ GeV}) = -43.73(64) \text{ MeV}, \quad (1)$$

$$f_{\gamma,d}^\perp(2 \text{ GeV}) = -44.45(74) \text{ MeV}, \quad (2)$$

$$f_{\gamma,s}^\perp(2 \text{ GeV}) = -51.0(1.8) \text{ MeV}, \quad (3)$$

which include the nonperturbative subtraction and multiplicative renormalization constants computed in the RI²-MOM scheme, cf. Ref. [28], and then converted to the $\overline{\text{MS}}$ scheme by using the 4-loop perturbative expressions available in Ref. [29].

¹In this approximation the ρ -meson pole saturates the sum in the expression given in Ref. [10], so that we have $\chi_\ell = -f_\rho f_\rho^T / (m_\rho \langle \bar{q}q \rangle)$. In the numerical evaluation we then use $\langle \bar{q}q \rangle = -(272(5) \text{ MeV})^3$ [13], and $f_\rho^T / f_\rho = 0.68(2)$ [14], as obtained in lattice QCD, together with $f_\rho^{\text{exp}} \simeq 208 \text{ MeV}$ and $m_\rho = 0.77 \text{ GeV}$ [15].

II. NORMALIZATION OF THE PHOTON DA AND ITS RELATION TO THE MAGNETIC SUSCEPTIBILITY OF THE QUARK CONDENSATE

Let us first consider the coupling of a photon to the tensor density $T_q^{\alpha\beta}(x, \mu) = Z_T(\mu) \bar{q}(x) \sigma^{\alpha\beta} q(x)$, and introduce $f_{\gamma,q}^\perp(p^2, \mu)$ as

$$\langle 0 | T_q^{\alpha\beta}(0, \mu) | \gamma(p^2, \varepsilon_\lambda) \rangle = i e_q f_{\gamma,q}^\perp(p^2, \mu) (\varepsilon_\lambda^\alpha p^\beta - \varepsilon_\lambda^\beta p^\alpha), \quad (4)$$

where ε_λ is the photon polarization, we use $\sigma^{\mu\nu} = (i/2)[\gamma^\mu, \gamma^\nu]$, and $e_q = e Q_q$ is the electric charge of the q -quark, with $e = \sqrt{4\pi\alpha_{\text{em}}}$, and $Q_u = +2/3$, $Q_{d,s} = -1/3$. Note that $Z_T(\mu)$ is the scale- and scheme-dependent renormalization constant of the tensor density. For a real photon $p^2 = 0$, $f_{\gamma,q}^\perp(0, \mu) \equiv f_{\gamma,q}^\perp(\mu)$ corresponds to the normalization of the q -quark contribution to the leading-twist photon DA [10].²

To leading order in the electromagnetic interaction, the matrix element defined in Eq. (4) can be expanded as³

$$\begin{aligned} \langle 0 | T_q^{\alpha\beta}(0, \mu) | \gamma(p^2, \varepsilon_\lambda) \rangle_{\text{QCD+QED}} \\ = i \int d^4x \langle 0 | T \{ T_q^{\alpha\beta}(0, \mu) J_\nu^{\text{em}}(x) A_\nu(x) \} | \gamma(p^2, \varepsilon_\lambda) \rangle + \mathcal{O}(\alpha_{\text{em}}^{3/2}) \\ = \varepsilon_{\lambda,\nu} H_q^{\alpha\beta\nu}(p) + \mathcal{O}(\alpha_{\text{em}}^{3/2}). \end{aligned} \quad (5)$$

where $J_\nu^{\text{em}} \equiv \sum_q e_q \bar{q} \gamma^\nu q$ is the electromagnetic current, and we introduced the hadronic tensor

$$H_q^{\alpha\beta\nu}(p) \equiv i \int d^4x e^{-ipx} \langle 0 | T \{ T_q^{\alpha\beta}(0, \mu) J_\nu^{\text{em}}(x) \} | 0 \rangle. \quad (6)$$

By virtue of Lorentz invariance the hadronic tensor $H_q^{\alpha\beta\nu}(p)$ can be written in terms of a single scalar form factor $H_q(p^2, \mu)$ as

$$\begin{aligned} H_q^{\alpha\beta\nu}(p) \equiv i \int d^4x e^{-ipx} \langle 0 | T \{ T_q^{\alpha\beta}(0, \mu) J_\nu^{\text{em}}(x) \} | 0 \rangle \\ \equiv i e_q H_q(p^2, \mu) (g^{\alpha\nu} p^\beta - g^{\beta\nu} p^\alpha), \end{aligned} \quad (7)$$

²To be more specific, $f_{\gamma,q}^\perp(\mu)$ is a factor multiplying the leading twist photon DA defined through the matrix element of a nonlocal operator (near light cone, $x^2 = 0$), namely

$$\begin{aligned} \langle 0 | \bar{q}(x) \sigma^{\alpha\beta} W_{-x}^x q(-x) | \gamma(p^2, \varepsilon_\lambda) \rangle \\ = i e_q \chi(\bar{q}q) (p^\beta \varepsilon_\lambda^\alpha - p^\alpha \varepsilon_\lambda^\beta) \int_0^1 du e^{ipx(2u-1)} \phi_\gamma(u), \end{aligned}$$

where W_x^γ is the Wilson line. In this way, the distribution is normalized as usual, $\int_0^1 du \phi_\gamma(u) = 1$, and $f_{\gamma,q}^\perp(\mu) = \chi(\mu) \langle \bar{q}q \rangle(\mu)$.

³Our choice of the sign is consistent with $D_\mu = \partial_\mu - i e_q A_\mu$, which is the same convention used in Ref. [10] for the covariant derivative.

so that, to leading order in the electromagnetic interaction, one arrives at $H_q(p^2, \mu) = f_{\gamma, q}^\perp(p^2, \mu)$.

The form factor $H_q(0, \mu)$ is also related to the zero-temperature magnetic susceptibility $\chi_q(\mu)$ of the quark condensate $\langle \bar{q}q \rangle(\mu)$. The latter is defined through the relation [10]

$$\langle 0 | T_q^{\alpha\beta}(0, \mu) | 0 \rangle_B \equiv F^{\alpha\beta} e_q \chi_q(\mu) \langle \bar{q}q \rangle(\mu), \quad (8)$$

where $F^{\alpha\beta} \equiv \partial^\alpha A^\beta - \partial^\beta A^\alpha$ is the electromagnetic field-strength tensor, corresponding to a constant weak background magnetic field B , and $\langle \dots \rangle_B$ means the expectation value evaluated in such a magnetic background field.

The connection between $H_q(0, \mu)$ and $\chi_q(\mu)$ can be easily worked out since

$$\begin{aligned} \langle 0 | T_q^{\alpha\beta}(0, \mu) | 0 \rangle_B &= i \int d^4x \langle 0 | T \{ T_q^{\alpha\beta}(0, \mu) J_{\text{em}}^\nu(x) \} | 0 \rangle A_\nu(x) \\ &+ \mathcal{O}(\alpha_{\text{em}}^{3/2}). \end{aligned} \quad (9)$$

Choosing $A_0 = 0, A_j = \varepsilon_{jk\ell} x^k B^\ell / 2$, where \vec{B} is the constant and uniform magnetic field, allows us to write, to leading order in the magnetic field,

$$\begin{aligned} \langle 0 | T_q^{\alpha\beta}(\mu) | 0 \rangle_B &= -\varepsilon_{jk\ell} \frac{B^\ell}{2} \frac{\partial}{\partial p_k} \int d^4x e^{-ipx} \langle 0 | T \{ T_q^{\alpha\beta}(0, \mu) J_{\text{em}}^j(x) \} | 0 \rangle_{p^2=0} \\ &= -e_q H_q(0, \mu) \varepsilon_{jk\ell} \frac{B^\ell}{2} [g^{\alpha j} g^{\beta k} - g^{\beta j} g^{\alpha k}] = e_q H_q(0, \mu) F^{\alpha\beta}, \end{aligned} \quad (10)$$

which, after a comparison with Eq. (8), gives $\chi_q(\mu) \langle \bar{q}q \rangle(\mu) = H_q(0, \mu) = f_{\gamma, q}^\perp(\mu)$. Similar expressions, relating $\chi_q(\mu)$ to current-current correlators have already been derived in Ref. [22], where the authors considered a rotating magnetic background field and the correlation function between the electromagnetic current (J_{em}) and the magnetic part, T_q^{ij} ($i \neq j$), of the tensor current.

A. Extracting $H_q(0, \mu)$ from Euclidean lattice correlators

To compute the form factor $H_q(0, \mu)$ we will be working in the so-called time-momentum representation and set $p = (p_0, 0, 0, 0)$. We can write

$$\frac{1}{3} \sum_{j=1}^3 H_q^{0jj}(p) = i \int_{-\infty}^{\infty} dt e^{-ip_0 t} \int d^3x \frac{1}{3} \sum_j \langle 0 | T \{ T_q^{0j}(0, \mu) J_{\text{em}}^j(\vec{x}, t) \} | 0 \rangle = i e_q H_q(p_0^2, \mu) p_0. \quad (11)$$

The crucial ingredient that makes this calculation possible is the observation that for small enough values of $|p_0|$ the previous expression can be analytically continued to Euclidean time without encountering any obstruction since QCD has a mass gap.⁴ For small $|p_0|$ we can thus write

$$-\frac{i}{3} \sum_j H_q^{0jj}(p) = e_q H_q(p_0^2, \mu) p_0 = - \int_{-\infty}^{\infty} dt e^{-p_0 t} C_q(t, \mu), \quad (12)$$

where $C_q(t, \mu)$ is the Euclidean lattice correlator

$$C_q(t, \mu) \equiv \frac{i}{3} \int d^3x \sum_j \langle 0 | T \{ T_q^{0j}(0, \mu) J_{\text{em}}^j(\vec{x}, t) \} | 0 \rangle_E, \quad (13)$$

and the subscript E indicates that the correlation function is evaluated in the Euclidean theory. The zero-momentum correlator, $C_q(t, \mu)$, is the nonperturbative object that we compute by means of QCD simulations on the lattice. Besides the finite constants needed to renormalize local vector currents on the lattice, the only scheme- and scale-dependent renormalization constant needed in this work is $Z_T(\mu)$ to which we will come back later on. In the following, for notational simplicity, we will drop out the renormalization scale dependence.

After taking the p_0 -derivative of both sides of Eq. (12) at $p_0 = 0$ we obtain the key expression

$$2 \int_0^\infty dt t C_q(t) = e_q H_q(0), \quad (14)$$

where we used the fact that $C_q(t)$ is odd under the Euclidean time reflection.

⁴The analytic continuation is possible for $|p_0| < E_0$, where E_0 is the energy of the lightest hadronic state propagating between the two currents. In QCD the threshold energy is $E_0 = 2M_\pi$.

Notice, however, that the expression (14) is well defined only in the chiral limit. For a nonzero quark mass, instead, the contact term between the tensor and electromagnetic currents generates a logarithmic divergence in Eq. (14) which must be properly subtracted away. The logarithmic divergence is present already in the free theory where the corresponding correlator $C_q^{\text{free}}(t)$, owing to the asymptotic freedom, is a good approximation of the full QCD correlator $C_q(t)$ only for very short time separations $t \ll \Lambda_{\text{QCD}}^{-1}$. The free theory calculation is discussed in detail in Appendix A. Here we only quote the final result, namely,

$$C_q^{\text{free}}(t) = -\text{sgn}(t) \frac{e_q N_c m_q^2}{2\pi^2 |t|} K_1(2m_q |t|) \underset{0 < t \ll m_q^{-1}}{\simeq} -\frac{e_q N_c m_q}{4\pi^2 t^2}, \quad (15)$$

where $K_1(x)$ is the modified Bessel function of the second kind. Since $C_q^{\text{free}}(t) \propto m_q/t^2$ at small times, the regularized time-integral develops a logarithmic divergence

$$2 \int_{\Lambda^{-1}}^{\infty} dt t C_q^{\text{free}}(t) \simeq e_q c_0 m_q \log(m_q/\Lambda) + \text{regular terms}, \quad (16)$$

with $c_0 = 2N_c/(2\pi)^2 \simeq 0.15$ for $N_c = 3$. In the lattice regularization, the ultraviolet cutoff Λ^{-1} is given by the lattice spacing a . In order to define the form factor $H_q(0)$ at nonzero quark mass, it is thus necessary to provide a prescription on how the logarithmic divergence is subtracted away. To this end we adopt a convenient prescription, described in Ref. [21], and define the subtracted (finite) form factor \bar{H}_q via

$$\bar{H}_q(0) = \left(1 - m_q \frac{\partial}{\partial m_q}\right) H_q(0). \quad (17)$$

Note that this prescription leaves the chiral limit unchanged, i.e.,

TABLE I. Parameters of the ETM ensembles used in this work: the light-quark bare mass, ($am_\ell = am_u = am_d$) and the corresponding pion mass (M_π), the lattice spacing (a), and the spatial size of lattice box L . The lattice spacing values are determined in a way explained in Appendix B of Ref. [26], i.e., by using $f_\pi^{\text{isoQCD}} = 130.4(2)$ MeV for the pion decay constant. We refer to [26] for more information regarding the statistics of the used ensembles.

Ensemble	β	$(L^3 \times T)/a^4$	a	am_ℓ	M_π	L (fm)
B64	1.778	$64^3 \times 128$	0.07957(13)	0.00072	140.2(0.2)	5.09
B96	1.778	$96^3 \times 192$	0.07957(13)	0.00072	140.2(0.2)	7.64
C80	1.836	$80^3 \times 160$	0.06821(13)	0.00060	136.7(0.2)	5.46
D96	1.900	$96^3 \times 192$	0.05692(12)	0.00054	140.8(0.2)	5.46

$$2 \int_0^\infty dt t \left[C_q(t) - m_q \frac{\partial}{\partial m_q} C_q(t) \right] = e_q \bar{H}_q(0). \quad (18)$$

As discussed in Refs. [21,22], the log-derivative will not only cancel the divergent contribution proportional to $m_q \log(am_q)$, but also the finite terms, proportional to powers of the quark mass m_q . The main result of this paper, which we are going to discuss in the next Sections, is the accurate determination of $\bar{H}_q(0)$ for the physical light ($q = u, d$) and strange ($q = s$) quarks, by making use of the gauge ensembles recently generated by the Extended Twisted Mass (ETM) Collaboration [24–27].

III. DETAILS OF THE COMPUTATION

Our results have been obtained by using the gauge field configurations generated by the ETM Collaboration employing the Iwasaki gluon action [30] and $N_f = 2 + 1 + 1$ flavors of Wilson-Clover twisted-mass fermions at maximal twist [23]. This framework guarantees the automatic $\mathcal{O}(a)$ improvement of on-shell parity-even quantities [31,32]. Basic information regarding the ensembles of gauge field configurations used in this work is collected in Table I. For more details the reader is referred to Refs. [24–27]. In Table II we give the values of the renormalization constants needed for the present work. The ensembles listed in Table I correspond to three values of the lattice spacing $a \in [0.056, 0.08]$ fm, and the size of the lattice box $L \in [5.09, 7.64]$ fm. The mass of the light sea-quarks has been tuned so as to give (almost) the physical pion mass. For all the ensembles, the strange and the charm sea-quarks are set to within about 5% of their physical masses, defined through the requirement that, cf. Refs. [25–27],

$$\frac{M_{D_s}}{f_{D_s}} = 7.9 \pm 0.1, \quad \frac{m_c}{m_s} = 11.8 \pm 0.2. \quad (19)$$

We work in a mixed-action framework in which the valence strange quark is discretized as an Osterwalder-Seiler fermion [32,33]. On each ensemble we evaluate the lattice correlator $C_s(t)$ for two different values of the

TABLE II. Renormalization constants (RCs) of the quark bilinear operators corresponding to the ETM ensembles of Table I. Z_V , Z_A , and Z_T stand for the RCs of the vector, axial and tensor operator, respectively. Z_T has been determined nonperturbatively in Ref. [28] in the $R'I''$ -scheme and then converted to the $\overline{\text{MS}}$. The scale independent renormalization constants Z_V and Z_A have been determined in Ref. [26] using the Ward identity method.

Ensemble	Z_V	Z_A	$Z_T^{\overline{\text{MS}}}(2 \text{ GeV})$
B64	0.706379(24)	0.74294(24)	0.847(1)(1)
B96	0.706405(17)	0.74267(17)	0.847(1)(1)
C80	0.725404(19)	0.75830(16)	0.863(1)(2)
D96	0.744108(12)	0.77395(12)	0.887(1)(2)

valence strange quark mass. The two simulated values, given in Table III, then allow us to interpolate to the physical strange quark mass which, as in Refs. [26,34], we define by requiring $M_{\eta_{ss'}} = 689.9(5)$ MeV [35], with $\eta_{ss'}$ being a fictitious pseudoscalar meson made of two mass degenerate quarks s and s' having mass equal to that of the strange quark. Besides the two valence strange quark masses, we employ a second value of the valence bare light quark mass, indicated in Table III as am'_ℓ , different from the sea light quark mass already given in Table I. For each flavor q , having results for (at least) two different

TABLE III. Values of the two bare strange-quark masses, am_s^L and am_s^H , and of the valence light quark mass am'_ℓ (see text for details), for each of the four ensembles of Table I.

Ensemble	am_s^L	am_s^H	am'_ℓ
B64	0.019	0.021	0.0006675
B96	0.019	0.021	0.0006675
C80	0.016	0.018	0.000585
D96	0.014	0.015	0.0004964

valence quark masses is necessary in order to compute the derivative $\partial C_q(t)/\partial m_q$ entering the definition of $\bar{H}_q(0)$ in Eq. (18), as we describe in the next section.

The Euclidean correlators $C_{q=u,d,s}(t)$ in Eq. (13) have been evaluated for the aforementioned valence quark masses for each of the ensembles listed in Table I. Note that $C_q(t)$ contains both a connected [$C_q^{\text{conn}}(t)$] and a disconnected [$C_q^{\text{disc}}(t)$] contribution. If we define the electromagnetic current as,

$$J_{\text{em}}^\mu(x) = \sum_{q'=u,d,s,c} J_{q'}^\mu(x), \quad J_{q'}^\mu(x) = e_{q'} \bar{q}'(x) \gamma^\mu q'(x), \quad (20)$$

we can write $C_q(t) = C_q^{\text{conn}}(t) + C_q^{\text{disc}}(t)$, with

$$\begin{aligned} C_q^{\text{conn}}(t) &= \frac{i}{3} \int d^3x \langle 0 | \text{T} \left\{ T_q^{0j}(0, \mu) J_q^j(\vec{x}, t) \right\} | 0 \rangle_E \\ &= \frac{e_q}{3} \int d^3x \langle \text{Tr} [\gamma^0 \gamma^j S_q(0, (\vec{x}, t)) \gamma^j S_q((\vec{x}, t), 0)] \rangle_U \end{aligned} \quad (21)$$

$$\begin{aligned} C_q^{\text{disc}}(t) &= \frac{i}{3} \int d^3x \langle 0 | \text{T} \left\{ T_q^{0j}(0, \mu) J_{\text{em}}^j(\vec{x}, t) \right\} | 0 \rangle_E \\ &= - \sum_{q'=u,d,s,c} \frac{e_{q'}}{3} \int d^3x \langle \text{Tr} [\gamma^0 \gamma^j S_q(0, 0)] \text{Tr} [\gamma^j S_{q'}((\vec{x}, t), (\vec{x}, t))] \rangle_U, \end{aligned} \quad (22)$$

where by $S_q(x, y)$ we denote the propagator of the q -quark, and $\langle \dots \rangle_U$ indicates the average over the SU(3) gauge field configurations, and the trace $\text{Tr}[\dots]$ is taken over the color and spin indices. The connected and disconnected contributions are sketched in Fig. 1. While the connected part $C_q^{\text{conn}}(t)$ receives the contribution from the q -quark component of the electromagnetic current, the disconnected diagram receives contributions from all quark flavors. The latter vanishes exactly in the SU(3) limit $m_u = m_d = m_s$ of the three-flavor theory, due to $e_u + e_d + e_s = 0$. In absence of

the disconnected contribution, the form factors $\bar{H}_u(0)$ and $\bar{H}_d(0)$ corresponding to the up- and down-quark are exactly equal. Indeed, for $m_u = m_d \equiv m_\ell$, one has $C_u^{\text{conn}}(t)/e_u = C_d^{\text{conn}}(t)/e_d$ [see also Eq. (14)]. The disconnected part of the correlator, for $m_u = m_d \equiv m_\ell$, satisfies instead $C_u^{\text{disc}}(t) = C_d^{\text{disc}}(t)$, which produces a shift of the form factor of the down quark which is two times larger (and opposite in sign) with respect to that of the up quark.

For the connected part, the inversions of the Dirac operator have been performed using $\mathcal{O}(10^3)$ and $\mathcal{O}(60)$

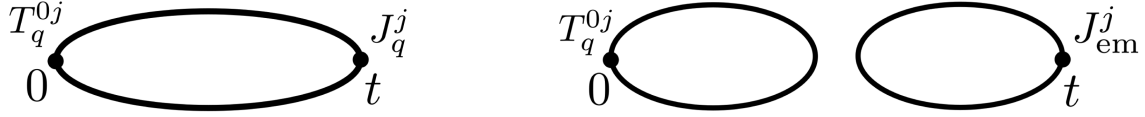


FIG. 1. Graphical representation of the quark-line connected (left diagram) and disconnected (right diagram) contributions to the Euclidean correlator $C_q(t)$.

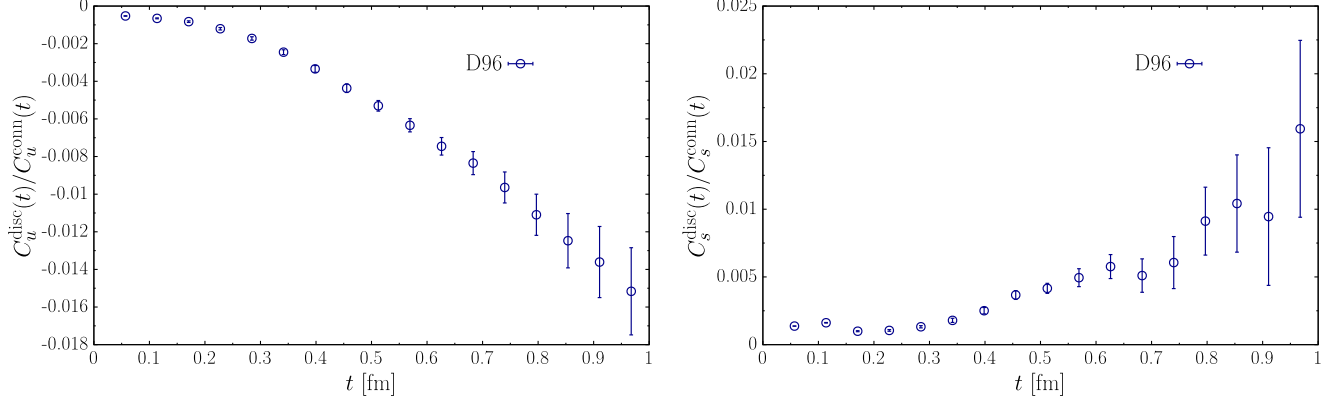


FIG. 2. Ratio between the disconnected [$C_q^{\text{disc}}(t)$] and connected [$C_q^{\text{conn}}(t)$] contributions to the correlator $C_q(t)$ for $q = u$ (left-plot) and $q = s$ (right-plot). The data correspond to the results obtained on the D96 ensemble.

stochastic sources, respectively for the light and the strange quarks. The sources are randomly distributed over time, diagonal in spin and dense in color. Various noise-reduction techniques are instead employed for disconnected loops. These are the one-end-trick [36], the exact deflation of low-modes [37], and hierarchical probing [38]. In contrast to the connected contribution, the disconnected loops have been computed using a single value of the valence quark mass for each of the $N_f = 2 + 1 + 1$ active quark flavors. For the light quarks u, d , this mass is equal to the sea quark mass am_ℓ , cf. Table I, while for the strange and charm quarks the simulated valence quark masses are obtained by tuning the Ω and Λ_c baryons to their physical values respectively. In Figure 2 we show the ratio between the disconnected [$C_q^{\text{disc}}(t)$] and connected [$C_q^{\text{conn}}(t)$] contributions to the correlator $C_q(t)$, for $q = u, s$. Clearly the disconnected contribution is orders of magnitude smaller than the connected one. After inspection, we find that the disconnected term produces a shift of the form factor $H_q(0)$ of order 0.5%, 1%, and 0.3%, respectively for $q = u, d$, and s .

Finally, another feature of our calculation is that the (completely dominant) connected part of the light- and strange-quark correlators are always evaluated employing two distinct discretized versions of the local tensor and vector currents given by,

$$T_q^{0j,\text{tm}} = Z_T(\mu)\bar{q}_+\gamma^0\gamma^j q_-, \quad J_q^{j,\text{tm}} = Z_A\bar{q}_+\gamma^j q_-, \quad (23)$$

$$T_q^{0j,\text{OS}} = Z_T(\mu)\bar{q}_+\gamma^0\gamma^j q_+, \quad J_q^{j,\text{OS}} = Z_V\bar{q}_+\gamma^j q_+, \quad (24)$$

where Z_A and Z_V are the (finite) renormalization constants of the axial and vector currents, which in twisted-mass QCD are chirally rotated with respect to the ones of the standard Wilson fermions. In the previous equation, the subscript \pm on the quark-fields, corresponds to a specific choice of the Wilson r -parameter (see e.g. [26] and references therein), given by

$$r_{q_\pm} = (-1)^\pm. \quad (25)$$

Since the twisted Wilson term, accompanied by the appropriate critical mass counterterm (for both sea and various valence quark fields), is a dimension-five irrelevant operator, the currents $T_q^{\text{tm}}, J_q^{\text{tm}}$ and $T_q^{\text{OS}}, J_q^{\text{OS}}$, when plugged into the expression (13), produce Euclidean correlators having the same continuum limit. Notice also that the label “tm” stands for twisted-mass and “OS” for Osterwalder-Seiler regularization. At finite lattice spacing, however, the two correlators are affected by different discretization effects, allowing one to approach the continuum limit from two different directions. The results shown in Figure 2 have been obtained by using C_q^{conn} in the “tm” regularization. In the following, we will present the results obtained using both the “tm” and the “OS” currents, which, as it will be discussed, can simultaneously be used to reach the continuum limit and achieve a better control of extrapolation. Moreover, we will oftentimes adopt the notation $X^{\text{tm(OS)}}$, to indicate that a given lattice observable X has been evaluated using the tm(OS) current. We emphasize once again that the values of Z_A and Z_V for each of our ensembles listed in Table I are provided in Table II.

A. Evaluating the derivative $\partial C_q(t)/\partial m_q$

We now discuss a delicate point regarding the derivative $\partial C_q(t)/\partial m_q$ for $q = u, d, s$. We start by splitting it to a valence- and a sea-quark contribution as

$$\frac{\partial C_q(t)}{\partial m_q} = \frac{\partial C_q(t)}{\partial m_q} \Big|_{\text{val}} + \frac{\partial C_q(t)}{\partial m_q} \Big|_{\text{sea}}. \quad (26)$$

In order to properly define the two contributions, we start from the path integral representation of a generic observable $\mathcal{O}(m_q)$. For the sake of simplicity and to avoid unnecessary complications, we consider the continuum action of a single quark field $q(x)$ of the bare quark mass, m_q , and we avoid explicitly writing the gauge field. We have

$$\langle \mathcal{O}(m_q) \rangle = \frac{1}{\mathcal{Z}(m_q)} \int [d\bar{q}dq] \exp \left\{ -S_0[\bar{q}, q] - m_q \int d^4x \bar{q}q(x) \right\} \mathcal{O}(\bar{q}, q, m_q), \quad (27)$$

where S_0 is the action in the massless limit and $\mathcal{Z}(m_q)$ is the partition function of the theory, i.e.,

$$\mathcal{Z}(m_q) \equiv \int [d\bar{q}dq] \exp \left\{ -S_0[\bar{q}, q] - m_q \int d^4x \bar{q}q(x) \right\}. \quad (28)$$

The expressions for the two terms on the right hand side of Eq. (26), read:

$$\frac{\partial \mathcal{O}(m_q)}{\partial m_q} \Big|_{\text{val}} \equiv \frac{1}{\mathcal{Z}(m_q)} \int [d\bar{q}dq] \exp \left\{ -S_0[\bar{q}, q] - m_q \int d^4x \bar{q}q(x) \right\} \frac{\partial}{\partial m_q} \mathcal{O}(\bar{q}, q, m_q) \equiv \left\langle \frac{\partial \mathcal{O}(m_q)}{\partial m_q} \right\rangle, \quad (29)$$

$$\begin{aligned} \frac{\partial \mathcal{O}(m_q)}{\partial m_q} \Big|_{\text{sea}} &\equiv \frac{1}{\mathcal{Z}(m_q)} \int [d\bar{q}dq] \frac{\partial}{\partial m_q} \left(\exp \left\{ -S_0[\bar{q}, q] - m_q \int d^4x \bar{q}q(x) \right\} \right) \mathcal{O}(\bar{q}, q, m_q) - \frac{\partial \ln \mathcal{Z}(m_q)}{\partial m_q} \langle \mathcal{O}(m_q) \rangle \\ &= - \int d^4x [\langle \bar{q}q(x) \mathcal{O}(m_q) \rangle - \langle \bar{q}q(x) \rangle \langle \mathcal{O}(m_q) \rangle]. \end{aligned} \quad (30)$$

Notice that the two contributions (29), (30) only involve the expectation values in the theory with a fixed sea-quark mass m_q , and therefore the derivative $\partial C_q(t)/\partial m_q$ can be computed without having to generate new gauge configurations at different values of the sea-quark masses. In summary, the valence contribution to the derivative can be evaluated from the slope of the observable $\mathcal{O}(m_q)$ with respect to the valence quark mass, while keeping the sea quark mass fixed. The sea quark contribution, instead, is given (up to a minus sign) by the gauge connected part of the correlation between the observable $\mathcal{O}(m_q)$ and the spacetime integral of the scalar density $\bar{q}q(x)$.

Bearing in mind Eqs. (29), (30) we can now discuss our calculation of $\partial C_q(t)/\partial m_q$. Given the smallness of the disconnected part, $C_q^{\text{disc}}(t)$, of the full correlator $C_q(t)$, we neglect in our calculations its contribution to the derivative $\partial C_q/\partial m_q$, considering only the contribution from the dominant connected part. We start by discussing the valence contribution to the derivative. If we denote by $m_q^{(L)}$ and $m_q^{(H)}$ the respective lowest and highest simulated valence quark masses for each flavor $q = u, d, s$, and by $C_q(t, m_q)$ the Euclidean correlator evaluated with a given

valence m_q (at the fixed simulated values of the sea-quark masses), we determine the valence contribution as,

$$\begin{aligned} \frac{\partial C_q(t)}{\partial m_q} \Big|_{\text{val}} &\simeq \frac{C_q(t, m_q^H) - C_q(t, m_q^L)}{\Delta m_q} + \mathcal{O}(\Delta m_q), \\ \Delta m_q &\equiv m_q^H - m_q^L. \end{aligned} \quad (31)$$

The simulated valence quark masses are ensured to satisfy $|\Delta m_q| \lesssim 0.1 m_q$ of the average mass, in both situations $q = u, d$ and $q = s$, cf. Tables I–III. Clearly, our evaluation of the valence contribution to the derivative using Eq. (31) is acceptable only if Δm_q is sufficiently small so that the higher order corrections to Eq. (31) are indeed negligible. We tested the validity of this assumption on a single ensemble (B64), and in the (more relevant) case of the strange quark contribution, by considering in addition to the valence masses given in Table III two more values, namely, $am_s = 0.018, 0.020$. We evaluated the derivative using all four masses and found that the typical error committed by estimating the derivative using Eq. (31) is about 2%, thus similar in size as our (total) statistical error of $\bar{H}_s(0)$. For that reason we attribute an additional 2% of systematic uncertainty to the strange quark mass derivative of the correlator evaluated

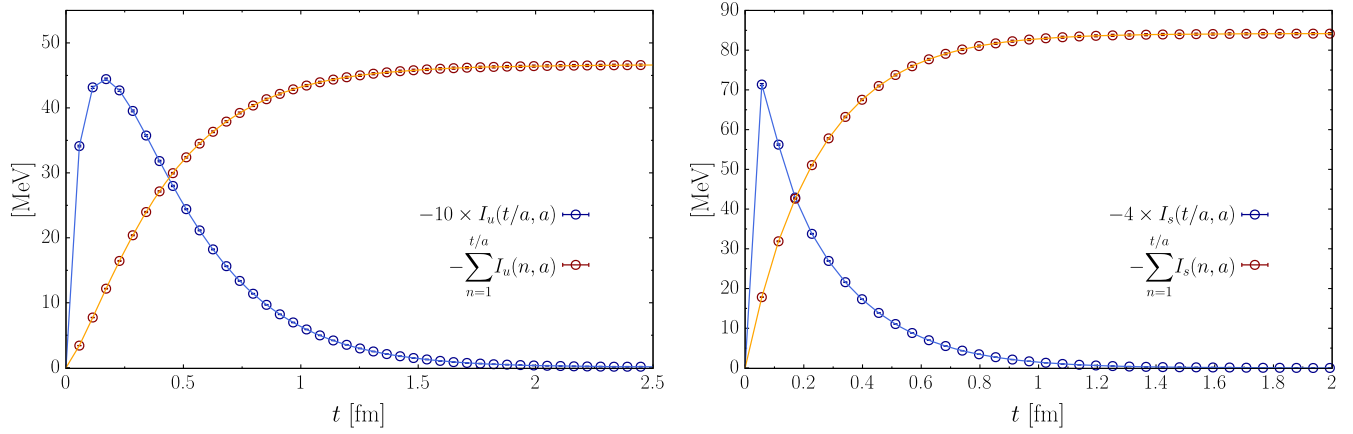


FIG. 3. The values of $I_q(n, a)$ (blue data points) and of its partial sums (red data points) on our finest lattice spacing ensemble and for the “tm” regularization. The left and right panels correspond to the cases $q = u$ and $q = s$, respectively. For the strange-quark contribution the results have been already interpolated to the physical strange quark mass.

using Eq. (31). In the case of the light quark contribution, instead, no additional systematic uncertainty is added, given that the contribution of the derivative for $q = u, d$ is approximately one order of magnitude smaller than for $q = s$, and this systematic effect is much smaller than the statistical error of our results.

In the case of the sea quark contribution to the derivative, we make use of Eq. (30) and of our determination of the light and strange scalar densities, to compute $\partial C_q(t)/\partial m_q|_{\text{sea}}$ using,

$$\left. \frac{\partial C_q(t)}{\partial m_q} \right|_{\text{sea}} = - \int d^4x [\langle \bar{q}q(x) C_q(t) \rangle - \langle \bar{q}q(x) \rangle \langle C_q(t) \rangle], \quad (32)$$

$q = u, d, s.$

It is important to notice that the product $m_q \partial/\partial m_q$ entering Eq. (18) is renormalization group invariant (RGI), hence Eqs. (31)–(32) can be evaluated using the bare quark masses and the bare scalar densities.

As it will be detailed in the numerical Section, the subtraction of the log-derivative in Eq. (18) has a much higher impact in the case of the strange-quark, where the contribution is enhanced due to the large quark-mass ratio $m_s/m_\ell \sim 27$ with respect to the case of the light quarks. In practice, it turns out that the subtraction is an order 5% effect in the case $q = u, d$, while it is of about 30%–40% in the case $q = s$.

IV. NUMERICAL RESULTS

We now turn to the results of our lattice calculation of $\bar{H}_q(0)$ for $q = u, d, s$. At finite lattice spacing we evaluate the (unsubtracted) form factor $H_q(0)$ from the knowledge of the correlator $C_q(na)$, with $n \in \{1, \dots, T/(2a)\}$, where T is the physical temporal lattice extent. We use the following discretized version of the integral (14),

$$H_q(0) = \sum_{n=1}^{n_{\max}} I_q(n, a) \equiv \sum_{n=1}^{n_{\max}} 2a^2 n \cdot C_q(na), \quad (33)$$

where $n_{\max} \leq T/2a$ is chosen large enough so that the sum in the previous equation already converged to its $n_{\max} \rightarrow \infty$ limit within errors. We optimize the value of n_{\max} so as to exclude from integration the contribution from the very large Euclidean times which only increase the noise in the resulting $H_q(0)$, but give no contribution to its signal. In the plots shown in Fig. 3 we illustrate the behavior of $I_q(n, a)$ and of its partial sums, for a selected gauge ensemble, the “tm” regularization, and for both the up- and the strange-quark contributions⁵ As it can be appreciated from the plots, the integrand $I_q(t/a, a)$ is peaked at very short time separations t , of the order of the lattice spacing, with the peak being more pronounced in the case of the strange quark. This is a manifestation of the logarithmic divergence affecting $H_q(0)$, which is expected to be more sizable for heavier quarks, and which we subtract away by using the prescription described above and specified in Eq. (18). To this purpose, we evaluate on each gauge ensemble the mass-derivative of the correlator $C_q(t)$ for $q = u, d, s$, using the procedure discussed in Sec. III A. We then compute the subtracted form-factor $\bar{H}_q(0)$ as,

$$\bar{H}_q(0) = \sum_{n=1}^{n_{\max}} \bar{I}_q(n, a) \equiv \sum_{n=1}^{n_{\max}} 2a^2 n \cdot \left[C_q(na) - m_q \frac{\partial C_q(na)}{\partial m_q} \right]. \quad (34)$$

⁵The down-quark contribution is very similar to the up-quark one. Their difference is proportional to the disconnected diagram in Fig. 1, which is two orders of magnitude smaller than the connected part.

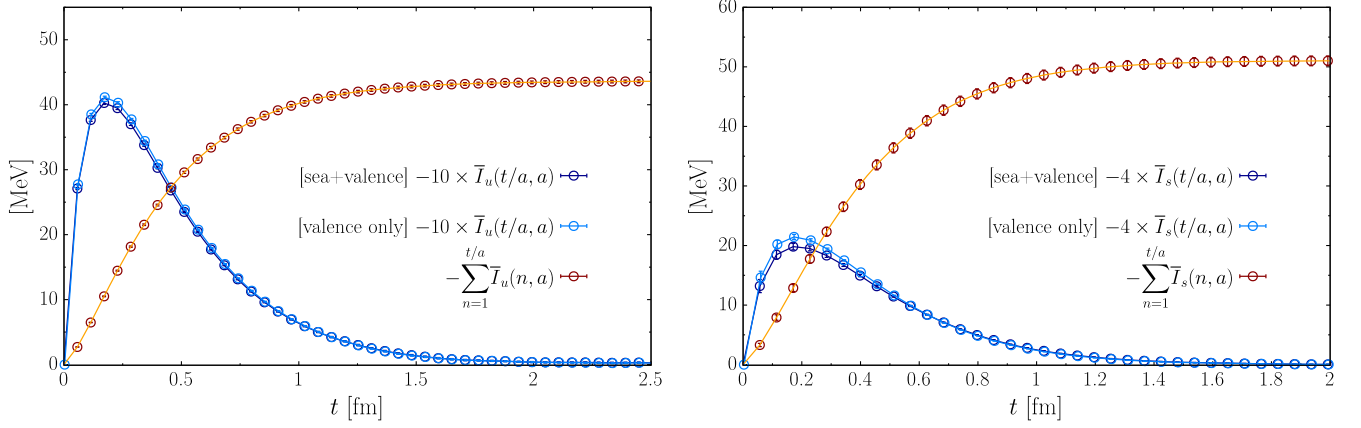


FIG. 4. The values of $\bar{I}_q(n, a)$ (blue data points) and of its partial sum (red data points) on our finest lattice spacing ensemble and for the “tm” regularization. The left and right figures correspond to the cases $q = u$ and $q = s$, respectively. For the strange-quark contribution the results have been already interpolated to the physical strange quark mass. The data points in light-blue correspond to the value of $\bar{I}_q(n, a)$ obtained neglecting the sea-quark contribution in Eq. (32) to the quark-mass derivative of the correlator.

The subtracted counterpart of Fig. 3 is shown in Fig. 4. The effect of the subtraction amounts to a $\mathcal{O}(5\%)$ shift of the form factor in the case of the up- and down-quark, while for the strange-quark, as expected, such an effect is much larger and the subtracted form factor $\bar{H}_s(0)$ is $\simeq 30\text{--}40\%$ smaller than the unsubtracted one, $H_s(0)$. In Fig. 4 we show separately the value of $\bar{I}_q(n, a)$ obtained by neglecting the sea quark contribution to the derivative [Eq. (32)]. While the sea quark contribution to the derivative is smaller than the valence one (by about one order of magnitude in the case of the strange-quark) it is non-negligible with respect to our current statistical accuracy. For that reason both terms in Eq. (26) should be and are taken into account. The results for the unsubtracted and subtracted form factors, $H_q(0)$ and $\bar{H}_q(0)$, for both regularization schemes and for $q = u, d, s$ are presented in Table IV.

We now move to the discussion of extrapolation of our lattice results both to the continuum ($a \rightarrow 0$) and to the infinite volume ($L \rightarrow \infty$).

A. Continuum and infinite-volume extrapolation

As described in the previous sections, we evaluated the (subtracted) form factors $\bar{H}_{u,d,s}(0)$ on the ensembles listed in Table I by using the “tm” and the “OS” regularizations. Apart from B96, all the ensembles from Table I have very similar spatial volumes. The ensembles C80 and D96 have (within uncertainties) the lattice extent $L \approx 5.46$ fm, while for the ensemble B64 it is slightly shorter, 5.09 fm. For the ensemble B96, instead, it is much larger, i.e., more than $L \approx 7.5$ fm. Our strategy to perform the combined extrapolation to the continuum and infinite volume limit can be summarized as follows. From the knowledge of the form factors on the ensembles B64 and B96 we interpolate $\bar{H}_q(0)$ at $\beta = 1.778$ to the reference lattice extent of $L_{\text{ref}} = 5.46$ fm. The interpolation is performed separately for the two regularizations (“tm” and “OS”), using a linear function in $\exp -M_\pi L$. In this way we can perform the continuum extrapolation at fixed volume $V_{\text{ref}} = L_{\text{ref}}^3$. We then associate to our extrapolated results at V_{ref} a systematic uncertainty $\Delta_L \bar{H}_q$ due to finite size effects (FSE’s),

TABLE IV. Results of the unsubtracted [$H_q(0)$] and subtracted [$\bar{H}_q(0)$] form factors obtained for each of the ensembles of gauge field configurations specified in Table I, for both the light nonstrange $q = u, d$ and the strange quark case $q = s$. As described in the text, we use two kinds of regularization schemes, denoted by “tm” and “OS”, and the form factor results are provided for both regularizations.

Ensemble	Form factor (MeV)	tm ($q = u$)	tm ($q = d$)	tm ($q = s$)	OS ($q = u$)	OS ($q = d$)	OS ($q = s$)
B64	$-H_q(0)$	46.59(15)	47.29(20)	78.98(18)	45.86(14)	46.58(20)	78.61(18)
	$-\bar{H}_q(0)$	43.65(21)	44.35(28)	51.01(75)	42.84(19)	43.56(26)	50.69(74)
B96	$-H_q(0)$	46.79(14)	47.51(19)	78.97(17)	46.05(13)	46.76(19)	78.59(17)
	$-\bar{H}_q(0)$	43.88(20)	44.60(28)	50.97(86)	43.28(23)	43.99(30)	50.64(85)
C80	$-H_q(0)$	46.23(17)	47.03(19)	81.00(18)	45.72(16)	46.52(19)	80.72(17)
	$-\bar{H}_q(0)$	43.44(33)	44.24(30)	50.18(86)	43.31(28)	44.12(28)	50.02(84)
D96	$-H_q(0)$	46.68(19)	47.38(24)	84.21(25)	46.28(20)	46.98(23)	84.00(24)
	$-\bar{H}_q(0)$	43.69(24)	44.38(28)	51.10(80)	43.35(26)	44.05(28)	50.95(79)

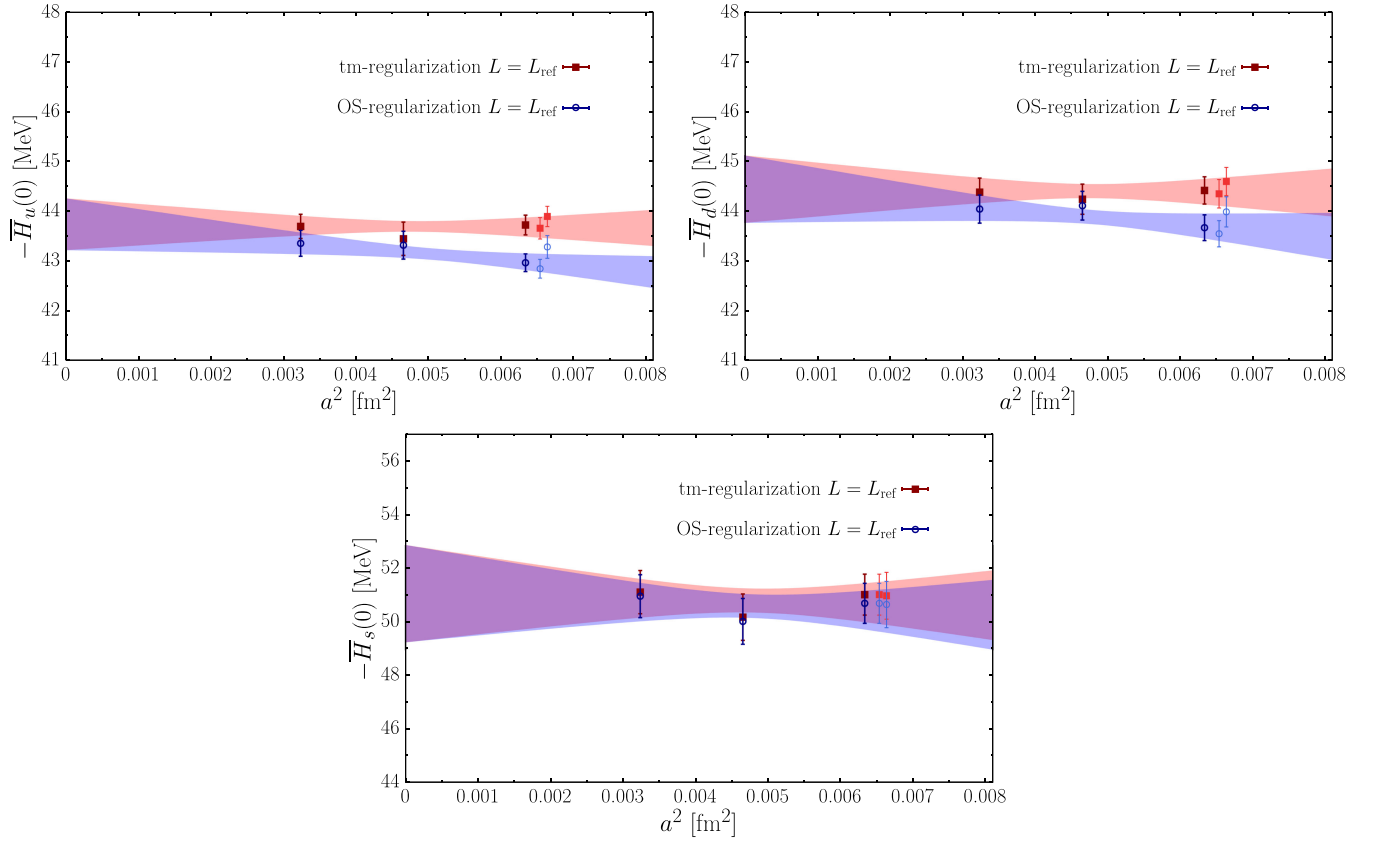


FIG. 5. Continuum limit extrapolation of $\bar{H}_u(0)$ (top-left panel), $\bar{H}_d(0)$ (top-right panel), and $\bar{H}_s(0)$ (bottom panel). The dark red and dark blue data points correspond to our results at $L = L_{\text{ref}}$ obtained by respectively using the ‘tm’ and ‘OS’ regularization. In order to highlight the typical size of the FSE’s we also show the raw data of the ensembles B64 and B96 (light red and light blue data points) at $a \simeq 0.079$ fm. Finally, the colored bands correspond to the best fit functions obtained in the continuum limit extrapolation using the ansatz (37).

which we estimate as

$$\Delta_L \bar{H}_q = \max_{r=\text{tm,OS}} \left\{ \Delta_q^r \text{erf} \left(\frac{\Delta_q^r}{\sqrt{2} \sigma_{\Delta_q^r}} \right) \right\}, \quad q = u, d, s, \quad (35)$$

where we have defined

$$\Delta_q^r = |\bar{H}_q^r(0, B96) - \bar{H}_q^r(0, B64)|, \quad (36)$$

and $\sigma_{\Delta_q^r}$ is its statistical uncertainty. The continuum extrapolation at $V = V_{\text{ref}}$ is carried out through a combined fit of the two regularizations (‘tm’ and ‘OS’) to the common continuum limit result, using the linear ansatz in a^2

$$\bar{H}_q^{\text{tm}}(0, a^2) = A_q + B_q^{\text{tm}} a^2, \quad \bar{H}_q^{\text{OS}}(0, a^2) = A_q + B_q^{\text{OS}} a^2, \quad q = u, d, s, \quad (37)$$

where A_q , B_q^{tm} and B_q^{OS} are the free fit parameters. We have minimized χ^2 which properly takes into account the correlation between the data obtained with ‘tm’ and

‘OS’ regularizations at the same value of β . The results of the combined continuum and infinite volume extrapolations are shown in the plots shown in Fig. 5. The red and blue data points correspond to the results obtained with two regularizations at $L = L_{\text{ref}}$, while the red and blue bands correspond to the best fit functions with a common continuum limit value. For both $\bar{H}_u(0)$, $\bar{H}_d(0)$ and $\bar{H}_s(0)$ the χ^2/N_{dof} of the fit is 0.6–0.7 with $N_{\text{dof}} = 3$. In order to highlight the typical size of the FSE’s we show in the same figure the raw data obtained on the B64 and B96 ensembles at $a \simeq 0.079$ fm. They are shown as light red and light blue data points for the ‘tm’ and ‘OS’ regularizations, respectively. A few comments are in order: First of all, the observed FSE’s are very small, completely negligible (within errors) for $\bar{H}_s(0)$, however similar in size to our statistical error for $\bar{H}_u(0)$ and $\bar{H}_d(0)$. Furthermore, the typical size of the cutoff effects is very modest and at most of the order of a few percent for both contributions. As it can be seen from the plots, the two regularizations give rise to very similar results already at our simulated values of the lattice spacing. This is different from what has been observed in the case of the correlation function of two

electromagnetic currents, $\langle J_{\text{em}} J_{\text{em}}^\dagger \rangle$, which enters the lattice calculation of the leading order hadronic vacuum polarization contribution to $(g-2)_\mu$ [26]. Our qualitative explanation of this feature is that, as shown by our tree level calculation in Appendix, the “tm” and “OS” tensor-vector

correlation functions coincide to all orders in $\mathcal{O}(\alpha_s^0 a^n m_q^r)$, and they only differ at order $\mathcal{O}(\alpha_s)$. This is not true for the vector-vector correlation function (see Appendix E of Ref. [26]). In the continuum and the infinite-volume limit, our final results in the $\overline{\text{MS}}$ scheme, read

$$\bar{H}_u(0, 2 \text{ GeV}) = f_{\gamma,u}^\perp(2 \text{ GeV}) = -43.73(52)_{L_{\text{ref}}(38)_{\text{FSE}}} \text{ MeV} = -43.73(64) \text{ MeV}, \quad (38)$$

$$\bar{H}_d(0, 2 \text{ GeV}) = f_{\gamma,d}^\perp(2 \text{ GeV}) = -44.45(67)_{L_{\text{ref}}(32)_{\text{FSE}}} \text{ MeV} = -44.45(74) \text{ MeV}, \quad (39)$$

$$\bar{H}_s(0, 2 \text{ GeV}) = f_{\gamma,s}^\perp(2 \text{ GeV}) = -51.0(1.8)_{L_{\text{ref}}(0)_{\text{FSE}}} \text{ MeV} = -51.0(1.8) \text{ MeV}, \quad (40)$$

where the first error corresponds to the total (statistical and systematic) error obtained after performing the continuum extrapolation at $L = L_{\text{ref}}$, and the second one to the estimate of the FSE’s obtained by using Eq. (35). Our results can be compared with those of Ref. [22], namely $f_{\gamma,u}^\perp(2 \text{ GeV}) \simeq f_{\gamma,d}^\perp(2 \text{ GeV}) = -45.4(1.5) \text{ MeV}$ and $f_{\gamma,s}^\perp(2 \text{ GeV}) = -68(5) \text{ MeV}$. While we find a good agreement with Ref. [22] for $f_{\gamma,u/d}^\perp$, we disagree by several standard deviations for $f_{\gamma,s}^\perp$. It must be noted that, in contrast to what is done in this work, the strange quark mass derivative of the form-factor $H_s(0)$, which is needed in order to cancel the logarithmic divergence of the unsubtracted form factor (18), has been estimated indirectly in Ref. [22], from the dependence of the form factor $H_{u/d}(0)$ on the light quark mass m_ℓ . Besides the observed discrepancy in the strange quark case, we obtain that the resulting uncertainties in both $\bar{H}_{u/d}(0)$ and $\bar{H}_s(0)$ are smaller than those quoted in Ref. [22] by a factor 2.3 and 2.8, respectively. That gain in precision does not translate to the precision of the value of susceptibility of the quark condensate. The reason is that the current value of $\langle \bar{q}q \rangle$ as extracted from the simulations with $N_f = 2 + 1$ dynamical flavors, $\langle \bar{q}q \rangle = -(272(5) \text{ MeV})^3$ [13], is more accurate than the one obtained from simulations with $N_f = 2 + 1 + 1$, $\langle \bar{q}q \rangle = -(286(23) \text{ MeV})^3$ [13]. By using the latter value we obtain $\chi_u^{\overline{\text{MS}}}(2 \text{ GeV}) = 1.87(45) \text{ GeV}^{-2}$ and $\chi_d^{\overline{\text{MS}}}(2 \text{ GeV}) = 1.90(46) \text{ GeV}^{-2}$. However, since the inclusion of the charm quark in the sea is very unlikely to affect the value of the quark condensate obtained from simulations with $N_f = 2 + 1$, we may as well use the $\overline{\text{MS}}$ value obtained from simulations with $N_f = 2 + 1$ at $\mu = 2 \text{ GeV}$, $\langle \bar{q}q \rangle = -(272(5) \text{ MeV})^3$ [13], which then leads to $\chi_u^{\overline{\text{MS}}}(2 \text{ GeV}) = 2.17(12) \text{ GeV}^{-2}$ and $\chi_d^{\overline{\text{MS}}}(2 \text{ GeV}) = 2.21(13) \text{ GeV}^{-2}$.

V. CONCLUSIONS

In this work we computed the normalization of the photon’s leading twist DA, $f_{\gamma,q}^\perp(0)$, by means of numerical

simulations of QCD with $N_f = 2 + 1 + 1$ dynamical quarks on the lattice. We rely on the gauge field configurations generated by the ETM Collaboration on which we compute the desired two-point correlation functions. We included the disconnected diagrams in our computation even though we verified that their contribution is orders of magnitude smaller than the connected ones. The additive and multiplicative renormalization is carried out fully nonperturbatively and then converted to the $\overline{\text{MS}}$ scheme by using the 4-loop perturbative matching.

By using two various lattice regularizations (denoted as “tm” and “OS” in the text) we were able to better control the extrapolation to the continuum limit. After a careful assessment of systematic uncertainties due to continuum extrapolation ($a \rightarrow 0$) and to the physical volume ($L \rightarrow \infty$) we find that the normalization of the leading twist DA of a photon coupling to u or d quark, in the $\overline{\text{MS}}$ renormalization scheme, is

$$f_{\gamma,u}^\perp(2 \text{ GeV}) = -43.73(64) \text{ MeV}, \quad (41)$$

$$f_{\gamma,d}^\perp(2 \text{ GeV}) = -44.45(74) \text{ MeV}, \quad (42)$$

while the coupling to the strange quark is,

$$f_{\gamma,s}^\perp(2 \text{ GeV}) = -51.0(1.8) \text{ MeV}. \quad (43)$$

Both results represent improvement with respect to the previous lattice QCD estimates. It was shown in Ref. [22] that $f_{\gamma,u/d}^\perp$ are indistinguishable from their values in the chiral limit, $\lim_{m_\ell \rightarrow 0} f_{\gamma,u/d}^\perp$. One can therefore deduce the value of the magnetic susceptibility of the quark condensate, $\chi_d \simeq \chi_u = f_{\gamma,u}^\perp / \langle \bar{q}q \rangle = 2.17(12) \text{ GeV}^{-2}$, where we used the FLAG value of $\langle \bar{q}q \rangle^{\overline{\text{MS}}}(2 \text{ GeV})$ obtained from simulations with $N_f = 2 + 1$ [13]. One would eventually prefer to use the condensate value from simulations with $N_f = 2 + 1 + 1$ but its current value is much less accurate, although its value is unlikely to change with respect to the $N_f = 2 + 1$ result.

ACKNOWLEDGMENTS

We thank all the members of the ETM Collaboration for the most enjoyable collaboration, the authors of Ref. [10] for correspondence, and of Ref. [22] for comments on the manuscript. We gratefully acknowledge CINECA and EuroHPC JU for giving this project access to Leonardo supercomputing hosted at CINECA. We acknowledge CINECA for the provision of GPU time under the specific initiative INFN-LQCD123 and IscrB_S-EPIC. F.S. and G.G are supported by the Italian Ministry of University and Research (MIUR) under Grant No. PRIN20172LNEEZ. F.S. and G.G. are supported by INFN under Grant No. GRANT73/CALAT. F.S. is supported by ICSC—Centro Nazionale di Ricerca in High Performance Computing, Big Data and Quantum Computing, funded by European Union—NextGenerationEU. S.B. has received funding from the European High-Performance Computing Joint Undertaking (JU) under Grant agreement No. 101118139. The JU receives support from the European Union’s Horizon Europe Programme. The authors gratefully acknowledge the Gauss Centre for Supercomputing e.V. for funding this project by providing computing time on the GCS Supercomputers SuperMUC-NG at Leibniz Supercomputing Centre and JUWELS [39] at Juelich Supercomputing Centre. The authors acknowledge the Texas Advanced Computing Center (TACC) at The University of Texas at Austin for providing HPC resources (Project ID PHY21001). The authors gratefully acknowledge PRACE for awarding access to HAWK at HLRS within the project with Id Acid 4886. We acknowledge the Swiss National Supercomputing Centre (CSCS)

and the EuroHPC Joint Undertaking for awarding this project access to the LUMI supercomputer, owned by the EuroHPC Joint Undertaking, hosted by CSC (Finland) and the LUMI consortium through the Chronos programme under project IDs CH17-CSCS-CYP and CH21-CSCS-UNIBE as well as the EuroHPC Regular Access Mode under project ID EHPC-REG-2021R0095. The open-source packages TMLQCD [40–43], LEMON [44], DD- α AMG [45–48], QPHIX [49,50] and QUDA [51–53] have been used in the ensemble generation.

APPENDIX: TREE-LEVEL CALCULATION OF $C_q(t)$

In this appendix we present the calculation of the free-theory correlator on the lattice, and obtain the relation appearing in Eq. (16). In the twisted-mass regularization, the momentum-space free-theory propagator of a quark-field ψ_q of mass m_q is given by

$$\langle \psi_q(p) \bar{\psi}_q(-p) \rangle = \frac{-i\gamma_\mu \tilde{p}_\mu + m_q + ir\gamma_5 \frac{a}{2} \sum_\mu \hat{p}_\mu^2}{\sum_\mu \tilde{p}_\mu^2 + m_q^2 + \frac{a^2}{4} (\sum_\mu \hat{p}_\mu^2)^2}, \quad (\text{A1})$$

where $r = \pm 1$ is the sign of the twisted Wilson term, the γ^μ are here the Euclidean gamma matrices ($\{\gamma^\mu, \gamma^\nu\} = 2\delta^{\mu\nu}$), and

$$\tilde{p}_\mu = \frac{1}{a} \sin(ap_\mu), \quad \hat{p}_\mu = \frac{2}{a} \sin\left(\frac{ap_\mu}{2}\right). \quad (\text{A2})$$

The coordinate-space quark propagator is then given by ($x_0 - y_0 = t$)

$$\langle \psi_q(x) \bar{\psi}_q(y) \rangle = \int_{-\frac{\pi}{a}}^{\frac{\pi}{a}} \frac{dp_0}{2\pi} \int_{-\frac{\pi}{a}}^{\frac{\pi}{a}} \frac{d^3\mathbf{p}}{(2\pi)^3} e^{ip_0 t} e^{i\mathbf{p}\cdot(\mathbf{x}-\mathbf{y})} \cdot \frac{-i\gamma_\mu \tilde{p}_\mu + m_q + ir\gamma_5 \frac{a}{2} \sum_\mu \hat{p}_\mu^2}{\sum_\mu \tilde{p}_\mu^2 + m_q^2 + \frac{a^2}{4} (\sum_\mu \hat{p}_\mu^2)^2}, \quad (\text{A3})$$

The integral over p_0 can be easily computed using the residue theorem. The denominator in Eq. (A1) can be written as

$$\sum_\mu \tilde{p}_\mu^2 + m_q^2 + \frac{a^2}{4} \left(\sum_\mu \hat{p}_\mu^2 \right)^2 = -\frac{2}{a^2} A(\mathbf{p}) (\cosh(ip_0) - \cosh(aE_p)), \quad (\text{A4})$$

where $A(\mathbf{p})$ and E_p are defined as

$$A(\mathbf{p}) = 1 + \frac{1}{2} a^2 \hat{\mathbf{p}}^2, \quad \cosh(aE_p) = 1 + \frac{a^2 B(\mathbf{p})}{2A(\mathbf{p})}, \quad B(\mathbf{p}) = m_q^2 + \hat{\mathbf{p}}^2 + \frac{a^2}{2} \sum_{i<j} \hat{p}_i^2 \hat{p}_j^2.$$

The momentum-space lattice quark propagator has two poles in the complex plane at $ip_0 = \pm E_p$, and the corresponding residue can be computed using

$$D^{-1}(\mathbf{p}) \equiv \lim_{ip_0 \rightarrow E_p} a^2 \frac{(ip_0 - E_p)}{2A(\mathbf{p})(\cosh(ip_0) - \cosh(aE_p))} = \frac{1}{\sqrt{B(\mathbf{p}) \cdot (4A(\mathbf{p}) + a^2 B(\mathbf{p}))}}. \quad (\text{A5})$$

Using the previous results, Eq. (A3) can be written for $t \neq 0$ as

$$\langle \psi_q(x) \bar{\psi}_q(y) \rangle = \int_{-\frac{\pi}{a}}^{\frac{\pi}{a}} \frac{d^3 \mathbf{p}}{(2\pi)^3} e^{-E_p |t|} \frac{e^{i\mathbf{p} \cdot (\mathbf{x}-\mathbf{y})}}{D(\mathbf{p})} \cdot \left[\text{sgn}(t) \frac{\gamma_0}{a} \sinh(aE_p) - i\boldsymbol{\gamma} \cdot \tilde{\mathbf{p}} + m_q + i r \gamma_5 \frac{a}{2} \left(\hat{\mathbf{p}}^2 - \frac{B(\mathbf{p})}{A(\mathbf{p})} \right) \right], \quad (\text{A6})$$

The free-theory vector-tensor lattice correlator

$$\begin{aligned} C_{\text{free},q}(t, a) &\equiv -\frac{ie_q}{3} \int d^3 \mathbf{x} \langle 0 | \text{Tr} \{ \bar{\psi}_q(0) \sigma^{0j} \psi_q(0) \bar{\psi}_q(\mathbf{x}, t) \gamma^j \psi_q(\mathbf{x}, t) \} | 0 \rangle, \\ &= -\frac{e_q}{3} \int d^3 \mathbf{x} \text{Tr} [\gamma^0 \gamma^j \langle \psi_q(0) \bar{\psi}_q(\mathbf{x}, t) \rangle \gamma^j \langle \psi_q(\mathbf{x}, t) \bar{\psi}_q(0) \rangle], \end{aligned} \quad (\text{A7})$$

where $\text{Tr}[\cdot]$ is intended over both color and Dirac indices, can be evaluated using Eq. (A6). The result is

$$C_{\text{free},q}(t, a) = -\frac{8e_q N_c}{(2\pi)^3} \text{sgn}(t) \int_{-\pi/a}^{\pi/a} d^3 \mathbf{p} e^{-2E_p |t|} (am_q) \frac{\sinh(aE_p)}{a^2 D^2(\mathbf{p})}. \quad (\text{A8})$$

It is interesting to notice that the dependence on the twisted-Wilson term completely disappeared, therefore at tree level the “tm” and “OS” regularization, which as already discussed in the main text differ by the relative sign of the parameter r between the forward and backward quark propagators, produce exactly the same result.

The continuum correlator can be then obtained through the replacement

$$\sinh(aE_p) \rightarrow aE_p \rightarrow a\sqrt{\mathbf{p}^2 + m_q^2}, \quad D^2(\mathbf{p}) \rightarrow 4(\mathbf{p}^2 + m_q^2), \quad (\text{A9})$$

so that one has

$$\begin{aligned} C_{\text{free},q}(t) &\equiv C_{\text{free},q}(t, 0) = -\frac{2e_q N_c}{(2\pi)^3} \text{sgn}(t) \int_{-\infty}^{\infty} d^3 \mathbf{p} e^{-2\sqrt{\mathbf{p}^2 + m_q^2} t} \frac{m_q}{\sqrt{\mathbf{p}^2 + m_q^2}} \\ &= -\frac{e_q N_c}{\pi^2} \text{sgn}(t) \int_0^{\infty} d|p| e^{-2\sqrt{|p|^2 + m_q^2} t} \frac{m_q |p|^2}{\sqrt{|p|^2 + m_q^2}} \\ &= -\frac{e_q N_c}{2\pi^2} \text{sgn}(t) \frac{m_q^2}{t} K_1(2m_q |t|), \end{aligned} \quad (\text{A10})$$

where $K_n(x)$ are the modified Bessel functions of the second kind. From the previous equation, using $K_1(x) = x^{-1} + \mathcal{O}(x)$, it is immediate to show the validity of Eq. (16).

-
- [1] I. I. Balitsky and A. V. Yung, Proton and neutron magnetic moments from QCD sum rules, *Phys. Lett.* **129B**, 328 (1983).
 - [2] B. L. Ioffe and A. V. Smilga, Nucleon magnetic moments and magnetic properties of vacuum in QCD, *Nucl. Phys.* **B232**, 109 (1984).
 - [3] M. A. Shifman, A. I. Vainshtein, and V. I. Zakharov, QCD and resonance physics. Theoretical foundations, *Nucl. Phys.* **B147**, 385 (1979).
 - [4] A. Czarnecki, W. J. Marciano, and A. Vainshtein, Refinements in electroweak contributions to the muon anomalous magnetic moment, *Phys. Rev. D* **67**, 073006 (2003).
 - [5] M. Pospelov and A. Ritz, Electric dipole moments as probes of new physics, *Ann. Phys. (Amsterdam)* **318**, 119 (2005).
 - [6] S. Narison, A fresh look into the neutron EDM and magnetic susceptibility, *Phys. Lett. B* **666**, 455 (2008).
 - [7] V. M. Braun, S. Gottwald, D. Y. Ivanov, A. Schafer, and L. Szymanowski, Exclusive photoproduction of hard dijets and magnetic susceptibility of QCD vacuum, *Phys. Rev. Lett.* **89**, 172001 (2002).
 - [8] P. Colangelo, F. De Fazio, and A. Ozpineci, Radiative transitions of $D^*(sJ)(2317)$ and $D(sJ)(2460)$, *Phys. Rev. D* **72**, 074004 (2005).
 - [9] J. Rohrwild, Determination of the magnetic susceptibility of the quark condensate using radiative heavy meson decays, *J. High Energy Phys.* **09** (2007) 073.
 - [10] P. Ball, V. M. Braun, and N. Kivel, Photon distribution amplitudes in QCD, *Nucl. Phys.* **B649**, 263 (2003).

- [11] I. V. Anikin and L. Szymanowski, Gluon poles and photon distribution amplitudes in Drell-Yan-like processes, *Eur. Phys. J. A* **54**, 130 (2018).
- [12] B. Pire and L. Szymanowski, Probing the nucleon's transversity and the photon's distribution amplitude in lepton pair photoproduction, *Phys. Rev. Lett.* **103**, 072002 (2009).
- [13] Flavour Lattice Averaging Group (FLAG) Collaboration, FLAG review 2021, *Eur. Phys. J. C* **82**, 869 (2022).
- [14] RBC, UKQCD Collaborations, $2 + 1$ flavor domain wall QCD on a $(2 \text{ fm})^3$ lattice: Light meson spectroscopy with $L(s) = 16$, *Phys. Rev. D* **76**, 014504 (2007).
- [15] Particle Data Group Collaboration, Review of particle physics, *Prog. Theor. Exp. Phys.* **2022**, 083C01 (2022).
- [16] A. Vainshtein, Perturbative and nonperturbative renormalization of anomalous quark triangles, *Phys. Lett. B* **569**, 187 (2003).
- [17] O. Cata, Relations between vacuum condensates and low energy parameters from a rational approach, *Phys. Rev. D* **81**, 054011 (2010).
- [18] P. V. Buividovich, M. N. Chernodub, E. V. Luschevskaya, and M. I. Polikarpov, Chiral magnetization of non-Abelian vacuum: A lattice study, *Nucl. Phys.* **B826**, 313 (2010).
- [19] V. V. Braguta, P. V. Buividovich, T. Kalaydzhyan, S. V. Kuznetsov, and M. I. Polikarpov, The chiral magnetic effect and chiral symmetry breaking in SU(3) quenched lattice gauge theory, *Phys. At. Nucl.* **75**, 488 (2012).
- [20] C. McNeile, A. Bazavov, C. T. H. Davies, R. J. Dowdall, K. Hornbostel, G. P. Lepage, and H. D. Trotter, Direct determination of the strange and light quark condensates from full lattice QCD, *Phys. Rev. D* **87**, 034503 (2013).
- [21] G. S. Bali, F. Bruckmann, M. Constantinou, M. Costa, G. Endrodi, S. D. Katz *et al.*, Magnetic susceptibility of QCD at zero and at finite temperature from the lattice, *Phys. Rev. D* **86**, 094512 (2012).
- [22] G. S. Bali, G. Endrődi, and S. Piemonte, Magnetic susceptibility of QCD matter and its decomposition from the lattice, *J. High Energy Phys.* **07** (2020) 183.
- [23] Alpha Collaboration, Lattice QCD with a chirally twisted mass term, *J. High Energy Phys.* **08** (2001) 058.
- [24] Extended Twisted Mass Collaboration, Quark masses using twisted-mass fermion gauge ensembles, *Phys. Rev. D* **104**, 074515 (2021).
- [25] Extended Twisted Mass Collaboration, Ratio of kaon and pion leptonic decay constants with $N_f = 2 + 1 + 1$ Wilson-clover twisted-mass fermions, *Phys. Rev. D* **104**, 074520 (2021).
- [26] C. Alexandrou *et al.*, Lattice calculation of the short and intermediate time-distance hadronic vacuum polarization contributions to the muon magnetic moment using twisted-mass fermions, *Phys. Rev. D* **107**, 074506 (2023).
- [27] C. Alexandrou *et al.*, Simulating twisted mass fermions at physical light, strange and charm quark masses, *Phys. Rev. D* **98**, 054518 (2018).
- [28] C. Alexandrou *et al.*, Moments of the nucleon transverse quark spin densities using lattice QCD, *Phys. Rev. D* **107**, 054504 (2023).
- [29] J. A. Gracey, Tensor current renormalization in the RI' scheme at four loops, *Phys. Rev. D* **106**, 085008 (2022).
- [30] Y. Iwasaki, Renormalization group analysis of lattice theories and improved lattice action: Two-dimensional nonlinear O(N) sigma model, *Nucl. Phys.* **B258**, 141 (1985).
- [31] R. Frezzotti and G. C. Rossi, Chirally improving Wilson fermions. I. O(a) improvement, *J. High Energy Phys.* **08** (2004) 007.
- [32] R. Frezzotti and G. C. Rossi, Chirally improving Wilson fermions. II. Four-quark operators, *J. High Energy Phys.* **10** (2004) 070.
- [33] K. Osterwalder and E. Seiler, Gauge field theories on the lattice, *Ann. Phys. (N.Y.)* **110**, 440 (1978).
- [34] R. Frezzotti, G. Gagliardi, V. Lubicz, G. Martinelli, F. Mazzetti, and C. T. Sachrajda, Lattice calculation of the D_s meson radiative form factors over the full kinematical range, *Phys. Rev. D* **108**, 074505 (2023).
- [35] S. Borsanyi *et al.*, Leading hadronic contribution to the muon magnetic moment from lattice QCD, *Nature (London)* **593**, 51 (2021).
- [36] UKQCD Collaboration, Decay width of light quark hybrid meson from the lattice, *Phys. Rev. D* **73**, 074506 (2006).
- [37] A. S. Gambhir, A. Stathopoulos, and K. Orginos, Deflation as a method of variance reduction for estimating the trace of a matrix inverse, *SIAM J. Sci. Comput.* **39**, A532 (2017).
- [38] A. Stathopoulos, J. Laeuchli, and K. Orginos, Hierarchical probing for estimating the trace of the matrix inverse on toroidal lattices, *SIAM J. Sci. Comput.* **35**, S299 (2013).
- [39] Jülich Supercomputing Centre, JUWELS cluster and booster: Exascale Pathfinder with modular supercomputing architecture at Juelich Supercomputing Centre, *J. Large-Scale Res. Facil.* **7**, A183 (2021), .
- [40] K. Jansen and C. Urbach, tmLQCD: A program suite to simulate Wilson twisted mass lattice QCD, *Comput. Phys. Commun.* **180**, 2717 (2009).
- [41] A. Abdel-Rehim, F. Burger, A. Deuzeman, K. Jansen, B. Kostrzewa, L. Scorzato *et al.*, Recent developments in the tmLQCD software suite, *Proc. Sci., LATTICE2013* (2014) 414 [arXiv:1311.5495].
- [42] A. Deuzeman, K. Jansen, B. Kostrzewa, and C. Urbach, Experiences with OpenMP in tmLQCD, *Proc. Sci., LATTICE2013* (2014) 416 [arXiv:1311.4521].
- [43] ETM Collaboration, Twisted mass ensemble generation on GPU machines, *Proc. Sci., LATTICE2022* (2023) 340 [arXiv:2212.06635].
- [44] ETM Collaboration, Lemon: An MPI parallel I/O library for data encapsulation using LIME, *Comput. Phys. Commun.* **183**, 1321 (2012).
- [45] A. Frommer, K. Kahl, S. Krieg, B. Leder, and M. Rottmann, Adaptive aggregation-based domain decomposition multigrid for the lattice Wilson-Dirac operator, *SIAM J. Sci. Comput.* **36**, A1581 (2014).
- [46] C. Alexandrou, S. Bacchio, J. Finkenrath, A. Frommer, K. Kahl, and M. Rottmann, Adaptive aggregation-based domain decomposition multigrid for twisted mass fermions, *Phys. Rev. D* **94**, 114509 (2016).
- [47] S. Bacchio, C. Alexandrou, and J. Finkerath, Multigrid accelerated simulations for twisted mass fermions, *EPJ Web Conf.* **175**, 02002 (2018).

- [48] C. Alexandrou, S. Bacchio, and J. Finkenrath, Multigrid approach in shifted linear systems for the non-degenerated twisted mass operator, *Comput. Phys. Commun.* **236**, 51 (2019).
- [49] B. Joó, D. D. Kalamkar, T. Kurth, K. Vaidyanathan, and A. Walden, Optimizing wilson-dirac operator and linear solvers for intel® knl, in *High Performance Computing: ISC High Performance 2016 International Workshops, ExaComm, E-MuCoCoS, HPC-IODC, IXPUG, IWOPH, P³MA, VHPC, WOPSSS, Frankfurt, Germany, 2016, Revised Selected Papers 31* (Springer, New York, 2016), pp. 415–427.
- [50] M. Schröck, S. Simula, and A. Strelchenko, Accelerating twisted mass LQCD with QPHIX, *Proc. Sci., LATTICE2015 (2016)* 030 [arXiv:1510.08879].
- [51] M. A. Clark, R. Babich, K. Barros, R. C. Brower, and C. Rebbi, Solving Lattice QCD systems of equations using mixed precision solvers on GPUs, *Comput. Phys. Commun.* **181**, 1517 (2010).
- [52] R. Babich, M. A. Clark, B. Joo, G. Shi, R. C. Brower, and S. Gottlieb, Scaling lattice QCD beyond 100 GPUs, in *SC11 International Conference for High Performance Computing, Networking, Storage and Analysis Seattle, Washington, 2011* (Association for Computing Machinery, New York, USA, 2011); arXiv:1109.2935.
- [53] M. A. Clark, B. Joó, A. Strelchenko, M. Cheng, A. Gambhir, and R. C. Brower, Accelerating lattice QCD multigrid on GPUs using fine-grained parallelization, in *SC '16: Proceedings of the International Conference for High Performance Computing, Networking, Storage and Analysis* (IEEE, 2016), pp. 795–806; arXiv:1612.07873.